A Thermo-Mechanically Coupled Large-Deformation Theory for Amorphous Polymers Across the Glass Transition Temperature

Proceedings of the ASME 2010 International Mechanical Engineering Congress & Exposition
IMECE2010
November 12-18, 2010, Vancouver, British Columbia, Canada

IMECE2010-37382

A THERMO-MECHANICALLY COUPLED LARGE-DEFORMATION THEORY FOR AMORPHOUS POLYMERS ACROSS THE GLASS TRANSITION TEMPERATURE

Shawn A. Chester, Vikas Srivastava, and Lallit Anand
Solid Mechanics and Materials Laboratory,
Department of Mechanical Engineering,
Massachusetts Institute of Technology,
Cambridge, Massachusetts 02139, USA

INTRODUCTION

Amorphous thermoplastic polymers are important engineering materials; however, their nonlinear, strongly temperature- and rate-dependent elastic-viscoplastic behavior is still not very well understood, and is modeled by existing constitutive theories with varying degrees of success. There is no generally agreed upon theory to model the large-deformation, thermo-mechanically-coupled, elastic-viscoplastic response of these materials in a temperature range which spans their glass transition temperature. Such a theory is crucial for the development of a numerical capability for the simulation and design of important polymer processing operations, and also for predicting the relationship between processing methods and the subsequent mechanical properties of polymeric products. In this manuscript we briefly summarize a few results from our own recent research [1–4] which is intended to fill this need.

We have conducted large strain compression experiments on three representative amorphous polymeric materials a cyclo-olefin polymer (Zeonex-690R), polycarbonate (PC), and poly(methyl methacrylate) (PMMA) in a temperature range from room temperature to approximately 50C above the glass transition temperature, ϑ_g, of each material, in a strain-rate range of roughly $0.0001\,\mathrm{s}^{-1}$ to $0.1\,\mathrm{s}^{-1}$, and compressive true strains exceeding 100%. We have specialized our constitutive theory to capture the major features of the thermo-mechanical response of the three materials studied experimentally.

We have numerically implemented our thermo-mechanically-coupled constitutive theory by writing a user material subroutine for a widely used finite element program Abaqus/Standard. In order to validate the predictive capabilities of our theory and its numerical implementation, we present the following validation experiments: (i) a plane-strain forging of PC at a temperature below ϑ_g, and another at a temperature above Tg; (ii) blow-forming of thin-walled semi-spherical shapes of PC above ϑ_g; and (iii) microscale hot-embossing of channels in PMMA above ϑ_g. By comparing the results from this suite of validation experiments of some key features, such as the experimentally-measured deformed shapes and the load-displacement curves, against corresponding results from numerical simulations, we show that our theory is capable of reasonably accurately reproducing the experimental results obtained in the validation experiments.

EXPERIMENTAL CHARACTERIZATION OF AMORPHOUS POLYMERS

Even though the mechanical behavior of polymers has been studied for a long time, comprehensive, pedigreed stress-strain data: (i) to large strains exceeding 100%, including *loading and unloading*; (ii) a variety of strain rates in the range $\approx 10^{-4}$ to 10^{-1} s^{-1}, achievable in modern servo-hydraulic testing machines; and (iii) a temperature range from room temperature to $\approx 50\,\mathrm{C}$ above the glass transition temperature for amorphous polymers, are not readily available, and are scattered in the literature.

In our work [2,3] we have generated such data by conducting

compression experiments on three important amorphous polymeric materials: Zeonex, PC, and PMMA. The nominal glass transition temperatures of these three materials are:

- Zeonex-690R: $\vartheta_g \approx 136\,\mathrm{C}$,
- PC: $\vartheta_g \approx 145\,\mathrm{C}$,
- PMMA: $\vartheta_g \approx 115\,\mathrm{C}$.

Our cylindrical compression test specimens were 12.7 mm diameter and 12.7 mm tall, and were annealed before and after machining to final shape by heating in a furnace at a temperature about 10 C above the glass transition temperature of each material, and holding at that temperature for two hours, before cooling to room temperature. The experiments were conducted using a servo-hydraulic Instron testing machine, fitted with a high-temperature furnace. Amorphous polymers are poor thermal conductors; accordingly, in order to heat the compression specimens uniformly, we also used heated steel compression platens in addition to the furnace. The platens were heated with cartridge heaters, and thermocouples inserted into each platen were used to control the temperature. The top compression platen also had an integrated spherical seat to help minimize any effects of misalignment during compression testing. To reduce friction at the platen/specimen interface, the platens were polished, and thin Teflon (PTFE) films were used as lubricating layers between the specimen and the platens. Before a given experiment, each specimen was allowed to anneal at the testing temperature for one hour prior to testing. The compression tests were carried out at constant *true strain-rates* to compressive true strains exceeding $\gtrapprox 100\%$; all strain measurements were made using an extensometer. The temperature and strain-rate ranges for each material were as follows:

(i) **Zeonex**: Temperature range: 25 C to 180 C. Strain-rates: 3×10^{-4}, 3×10^{-3}, 3×10^{-2}, and $3\times10^{-1}\ \mathrm{s}^{-1}$.
(ii) **PC**: Temperature range: 25 C to 175 C. Strain-rates: 10^{-3}, 10^{-2}, and $10^{-1}\ \mathrm{s}^{-1}$.
(iii) **PMMA**: Temperature range: 25 C to 170 C. Strain-rates: 3×10^{-4}, 10^{-3}, 10^{-2}, and $10^{-1}\ \mathrm{s}^{-1}$.

Figure 1 shows representative true stress-strain curves for Zeonex a strain-rate of $3\times10^{-4}\,\mathrm{s}^{-1}$ at temperatures ranging from 25 C through 160 C, while Figure 2 shows a set of stress-strain curves for Zeonex at strain rates of 3×10^{-4}, 3×10^{-3}, 3×10^{-2}, and $3\times10^{-1}\ \mathrm{s}^{-1}$ and temperatures of 25 C and 160 C.

Referring to Figure 1a, that is for temperatures less than $\vartheta_g \approx 136\,\mathrm{C}$, we see that in the glassy region:

(i) The stress-strain curves exhibit a well-defined yield-peak, followed by strain-softening, and eventual strain-hardening at large strains due to the limited extensibility of the polymer chains.

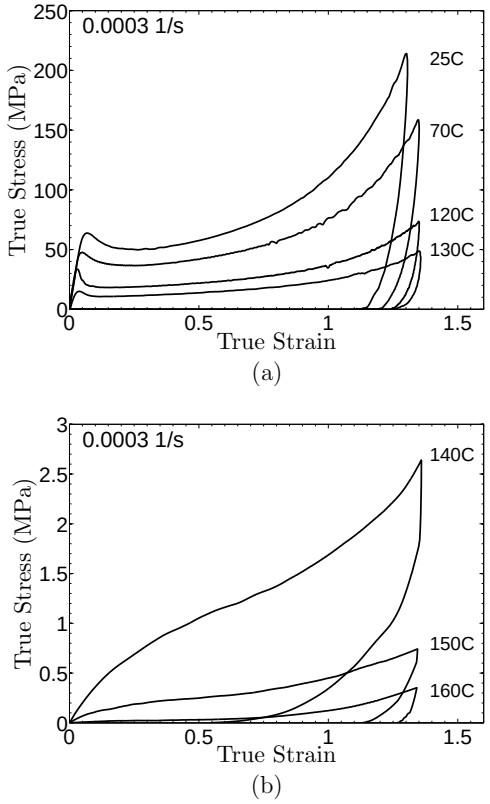

Figure 1. Stress-strain curves in simple compression for Zeonex at various temperatures ranging from 25 C to 160 C at a strain rate of 0.0003 1/s: (a) for temperatures below ϑ_g, and (b) for temperatures above ϑ_g. Note the change in scale for the two figures.

(ii) As the temperature increases in the glassy region from 25 C to 130 C, the magnitude of the yield-peak diminishes, the yield strength decreases with temperature from ≈ 65 MPa to ≈ 15 MPa, and the amount of strain-hardening observed at large strains diminishes.
(iii) Upon unloading after compression to strains exceeding 125%, approximately 5% of the strain is recovered, and there is permanent-set.

In contrast, referring to Figure 1b, we see that above the glass transition temperature:

(i) The initial stiffness of the material has dropped dramatically.
(ii) The yield-peak has disappeared.
(iii) The stress-strain response during the loading-phase is highly non-linear and exhibits strain-hardening. However, the stress levels at large strains are below 3 MPa at 140 C, and no more than 0.5 MPa at 160 C.
(iv) Upon unloading after compression to strains exceeding 125%, the material exhibits a highly non-linear unloading response and significant permanent-set. The amount of

permanent-set increases dramatically as the temperature increases form 140 C to 160 C.

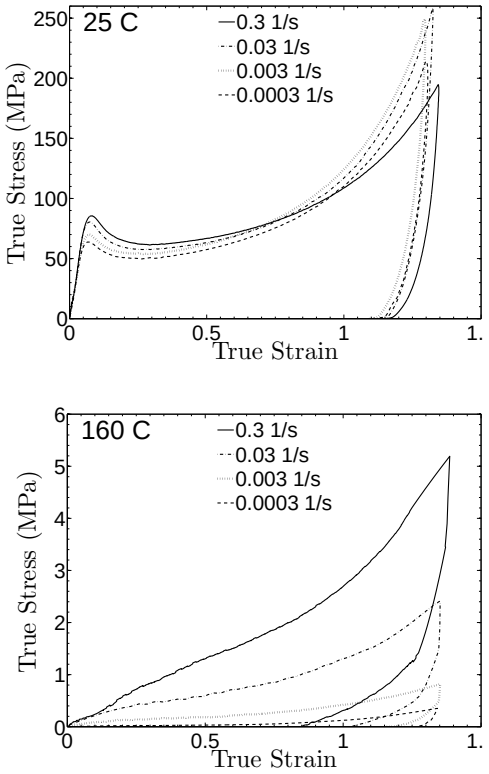

Figure 2. Stress-strain curves in simple compression for Zeonex at strain rates of 0.3, 0.03, 0.003, and 0.0003 1/s at temperatures of 25 C and 160 C. Note the change in scale between the two figures.

Referring to Figure 2 which shows stress-strain curves for Zeonex at two fixed temperatures and four different strain rates, we see obvious strain-rate dependent features of the material response. In the low-temperature glassy region, $\vartheta < 136\,\mathrm{C}$, the yield strength of the material increases by about 10% for a one-decade increase in strain-rate at any given temperature. Another important strain-rate dependent feature is the softening observed at large strains at the highest strain rate of 3×10^{-1} s $^{-1}$ at temperatures of 25 C, 70 C and 120 C. This softening is attributable to (near) "adiabatic" heating at the high strain rates. Significant strain rate sensitivity can also be observed at temperatures above the glass transition temperature, and similar to the behavior below glass transition, the stress levels are higher for higher strain rates.

A complete set of stress-strain curves for Zeonex, PC, and PMMA are presented in [2, 3] and are not included here for brevity.

SUMMARY OF THE CONSTITUTIVE THEORY

For brevity we do not give a detailed development of our theory, but only summarize the major governing constitutive and field equations. The details of the constitutive theory are presented in [1–3].

An essential kinematical ingredient of elastic-viscoplastic constitutive theories for amorphous polymers *below their glass transition temperatures*, is the classical multiplicative decomposition

$$\mathbf{F} = \mathbf{F}^e\mathbf{F}^p, \quad \text{with} \quad \det\mathbf{F}^e > 0 \quad \text{and} \quad \det\mathbf{F}^p > 0, \qquad (1)$$

of the deformation gradient $\mathbf{F}$ into elastic and plastic parts $\mathbf{F}^e$ and $\mathbf{F}^p$ [1, 5–7]. Since we wish to model the behavior of glassy polymers in the technologically important temperature range which *spans their glass transition temperatures*, and since the number of *microscopic relaxation mechanisms* in these polymers increases as the temperature is increased, we base our theory on a "multimechanism" generalization of the decomposition (1),

$$\left.\begin{aligned} &\mathbf{F} = \mathbf{F}^{e(\alpha)}\mathbf{F}^{p(\alpha)}, \quad \text{with} \quad \det\mathbf{F}^{e(\alpha)} > 0, \\ &\text{and} \quad \det\mathbf{F}^{p(\alpha)} > 0, \quad \alpha = 1,\ldots,M, \end{aligned}\right\} \qquad (2)$$

where each α denotes a local micromechanism of deformation. Such a multi-mechanism generalization forms the basis of the work of Buckley, Boyce, and their co-workers [8–11]. For each micromechanism indexed by α, we refer to $\mathbf{F}^{p(\alpha)}$ and $\mathbf{F}^{e(\alpha)}$ as the *plastic and elastic parts* of $\mathbf{F}$.

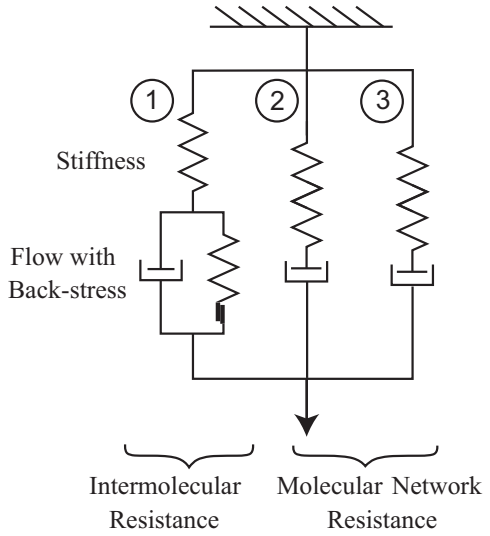

Figure 3. A schematic spring-dashpot-representation of the constitutive model.

The fewer the "number of micromechanisms," M, which are needed to phenomenologically describe the response of a material, then the fewer the number of "material parameters" that are needed to flesh-out the constitutive theory. In our previous study on modeling the response of amorphous polymers below ϑ_g, we found that a theory with $M = 2$ was quite adequate [1,2]. In order to model the response of these materials, which extends to temperatures which are approximately 50 C above ϑ_g, we find that we need to increase the number of micromechanisms to $M = 3$. Although no real material is composed of springs and dashpots, as a visual aid, Figure 3 shows a schematic "spring-dashpot"-representation of these three micromechanisms:

(i) **The first micromechanism ($\alpha = 1$)**: (a) The nonlinear spring represents an "elastic" resistance to intermolecular (and perhaps intramolecular) energetic bond-stretching. (b) The dashpot represents thermally-activated plastic flow due to "inelastic mechanisms," such as chain-segment rotation and relative slippage of the polymer chains between neighboring mechanical cross-linkage points. (c) The nonlinear spring in parallel with the dashpot represents an "energy storage" mechanism due to the local elastic incompatibilities caused by the viscoplastic flow mechanisms. We introduce a defect energy only for micromechanism $\alpha = 1$, via an internal variable; even for this micromechanism, the role of such a stored energy decreases as the molecular mobility increases when the temperatures approach and exceed ϑ_g.

(ii) **The second and third micromechanisms ($\alpha = 2,3$)**: (a) The nonlinear springs represent resistances due to changes in the free energy upon stretching of the molecular chains between the mechanical cross-links. (b) The dashpots represent thermally-activated plastic flow due to slippage of the "mechanical" cross-links, which are relatively strong below ϑ_g, but are progressively destroyed at temperatures above ϑ_g. The fact that we employ two such mechanisms is necessitated by the experimentally-observed increased complexity of the response of amorphous polymers as the temperature transitions across the range of temperatures from below ϑ_g to sufficiently above ϑ_g. We neglect any defect energies associated with mechanisms $\alpha = 2,3$.

Our strategy to phenomenologically model the response of the material as the temperature is increased to ϑ_g and beyond, is as follows:

- For temperatures $\vartheta < \vartheta_g$, *we do not allow any plastic flow in the dashpots associated with micromechanisms* $\alpha = 2$ and $\alpha = 3$. Thus, since the springs in $\alpha = 2$ and $\alpha = 3$ are in parallel, for all practical purposes the three-micromechanism model reduces to a simpler two-micromechanism model, which we have recently successfully used to model the response of amorphous polymers for temperatures $\vartheta < \vartheta_g$ [1,2].
- For temperatures $\vartheta > \vartheta_g$, we allow for plastic flow in the dashpots associated with micromechanisms $\alpha = 2$ and $\alpha = 3$, but *quickly drop the plastic flow resistance in mechanism* $\alpha = 2$ *to a very small value*, so that for all practical purposes in this temperature range, only mechanisms $\alpha = 1$ and $\alpha = 3$ contribute to the macroscopic stress.

Remark: At first blush it might appear possible to combine mechanisms $\alpha = 2$ and $\alpha = 3$ into a single micromechanism, say $\alpha = 2$, and simply make the modulus associated with the spring in this single branch to be strongly *temperature-dependent* — taking on high values below ϑ_g and low values above ϑ_g. However, this would lead to *incorrect* predictions concerning the amount of "elastic recovery" in circumstances where the polymer is first heated to a temperature above ϑ_g, subjected to a large deformation which includes large stretching of the spring, and then cooled to below ϑ_g under traction boundary conditions. Thus, since by assumption the modulus associated with spring in the single additional branch $\alpha = 2$ increases with decreasing temperature, the amount of "elastic recovery" (spring-back) upon cooling under traction boundary conditions would be unphysically too large. Conversely, cooling under displacement boundary conditions, would result in large residual stresses.

VALIDATION EXPERIMENTS AND SIMULATIONS

In this section we show the results of some validation experiments (which were not used to calibrate the material parameters of the theory), and compare the results against corresponding simulations. Here, for brevity, we only give a brief sketch of some of the validation experiments and simulations which are presented in [2, 3].

Plane-strain forging of PC

Plane-strain forging experiments at 25 C and 160 C, under isothermal conditions, were performed on PC specimens ($\vartheta_g \approx$ 145 C). The forging operation converts a cylindrical specimen with a circular cross-section into a specimen with a cross-section which is in the shape of a cruciform. The PC forging specimens had an original diameter of 12.7 mm, and were 12.7 mm deep in the plane-strain direction. The split-dies which impart the cruciform shape to the workpiece, were made from hardened tool steel. For the experiment conducted at 25 C the interfaces between the workpiece and the dies were lubricated to minimize frictional effects; however, no lubrication was used for the experiment conducted at 160 C due to degradation of the lubricant at high temperatures. The forging experiments were carried out under displacement control to a relative die-displacement of 4.6 mm at a constant die-closing velocity of 0.02 mm/s, and then the die motion was reversed at the same absolute velocity to unload the specimen. After unloading, the specimen which was forged at 160 C was immediately air-cooled to room temperature.

For the finite element simulation of the forging process we made use of the symmetry of the geometry, and only meshed one-quarter of the geometry. The quarter-circle of the workpiece cross-section was meshed using 277 ABAQUS-CPE4HT thermo-mechanically coupled elements, and the cruciform-die was modeled as a rigid surface. For the experiment at 25 C the workpiece was well-lubricated, and therefore the contact between the die and the workpiece was modeled as frictionless. However, since no lubrication was applied in the experiment at 160 C, the contact between the die and the workpiece was modeled as frictional, with a high Coulomb friction coefficient of 0.75

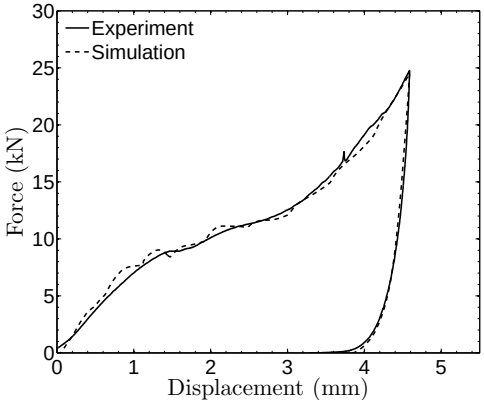

(a)

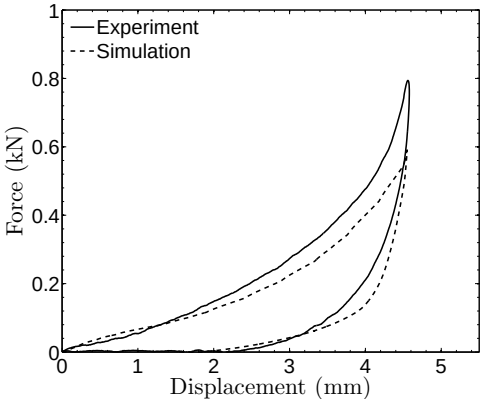

(b)

Figure 4. Comparison of the numerically-predicted and experimentally-measured force-displacement curves for forgings of PC at (a) 25 C and (b) 160 C. Note the change in scale between the two figures.

Figure 4a and Figure 4b compare the numerically-predicted and experimentally-measured, load-unload force versus displacement curves for the forging processes at 25 C and 160 C, respectively. The numerical simulations are able to reasonably accurately predict load-displacement behaviors at both 25 C, which is well below ϑ_g , as well as at 160 C, which is 15 C higher than ϑ_g of PC. Note that the maximum force for forging at 25 C is 25kN, while the maximum force for forging at 160 C is only 0.8 kN.

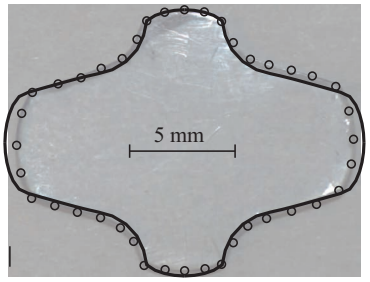

25 C

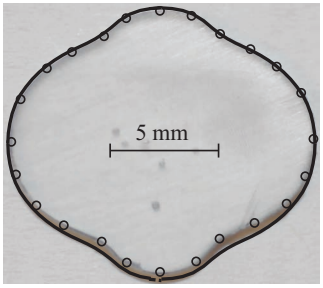

160 C

Figure 5. Comparison of the numerically-predicted and experimentally-measured deformed shapes from the cruciform forgings at 25 C (top) and 160 C (bottom). The solid lines are the edge-geometries from the numerical simulations, and the circles outline the geometry of the specimen from the experiment.

At the end of the loading process, with the dies still closed, the polycarbonate specimens conform with the shape of the cruciform forging dies. Upon die retraction and unloading, the polycarbonate specimens undergo some shape-recovery. For the forging experiment conducted at 25 C there is only a little shape-recovery after unloading, while for the forging experiment conducted at 160 C there is significant shape-recovery after unloading. After unloading, and cooling down to room temperature, each forged specimen was sectioned, polished, and photographed. Figure 5 compares the experimentally-measured and numerically-predicted deformed shapes after unloading, die removal, and cooling for the forgings conducted at 25 C and 160 C, respectively. For both cases the numerically-predicted final geometry is in reasonably good agreement with that which is experimentally-measured.

Blow-forming of PC

Next, we consider blow-forming of flat PC sheets into thin-walled semi-spherical shapes above ϑ_g . The starting circular blanks, 102 mm in diameter, were machined from 3 mm thick PC sheets. The blanks were clamped in a blow-forming fixture; the bottom part of the fixture was essentially a 50 mm diameter thick-walled cylinder which was attached to a high-pressure regulated air-supply, and the top clamping plate contained a 50 mm diameter hole for the polymer to freely expand under pressure. The experiments were performed under two different processing conditions: (i) at 155 C under a forming pressure of 20 psi (0.14 MPa), and (ii) at 160 C under a pressure of 35 psi (0.24 MPa). The forming process consists of four steps: (a) heating from room temperature to the processing temperature over a period of 10 min; (b) ramping the pressure to the processing pressure in 2 min; (c) holding at the processing-pressure while simultaneously cooling back to room temperature in 15 min; and (d) finally relieving the pressure.

For the finite element simulation of such a process, we make use of the axial-symmetry of the geometry, and mesh only a slice of the geometry. The polymer sheet is modeled using 252 ABAQUS-CAX4HT axi-symmetric, thermo-mechanically-coupled elements with 5 elements through the sheet thickness. The clamps are modeled as rigid surfaces, and the surface-interaction between the workpiece and the clamps is modeled as frictional, with a high Coulomb friction coefficient of 0.9.

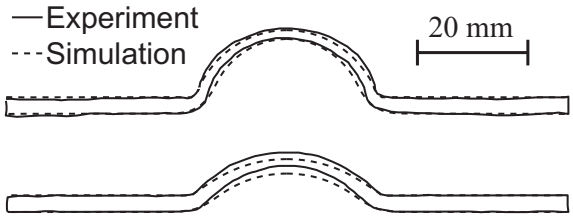

Figure 6. Comparison of the numerically-predicted profiles (dashed lines), against corresponding experimentally-measured traced surface profiles (solid lines): (top) 160 C and 35 psi, and (bottom) 155 C and 20 psi.

Figure 6 shows a comparison of the experimentally-measured profiles of the specimen cross-sections (solid lines), against corresponding numerically-predicted profiles (dashed lines): the figure at the top is for blow-forming at 160 C and 35 psi, and that at the bottom is for blow-forming at 155 C and 20 psi. The predictions of the bulged-shapes from the simulations are in good agreement with the experiments.

Micron-scale hot-embossing of PMMA

Of major importance for creating micron-scale surface features (such as capillary channels for microfluidic chips) in polymeric substrates is the replication method of micro-hot-embossing. The basic process of micro-hot-embossing is as follows: the polymeric substrate is heated to 10-30 C above its glass transition temperature and a rigid stamp containing micron scale features is pressed into the heated polymer to allow the polymer to flow and fill the cavities, transferring the features in the tool to the polymeric substrate. Pressure is then held and the system is cooled to the demolding temperature (typically 20-60 C below the glass transition temperature), and the tool is removed from the polymer part.

In this example we consider embossing a series of long channels into a PMMA substrate at an embossing temperature of 130 C, at three different embossing pressures – 0.48 MPa, 1.12 MPa, and 1.6 MPa. Three different embossing pressures of increasing magnitude were considered in order to compare the numerically-predicted and experimentally-measured partially embossed geometries.

The pattern consists of channels which are 65 μm wide, 27 μm deep, and spaced 123 μm apart. A 25 mm square, 1 mm thick sheet of PMMA, and a slightly larger patterned silicon tool were aligned and placed between heated compression platens. In the hot-embossing experiments the tool and polymer were brought into contact and then heated to the embossing temperature of 130 C. After reaching the embossing temperature, the load was ramped to produce the desired nominal embossing pressure at a constant rate of 0.15 MPa s^{-1}. After which the polymer and tool were cooled over 10 minutes to the demolding temperature of 90 C and the pressure was removed. For the corresponding numerical simulations, we employ a plane-strain idealization and consider only a single half-segment with suitable periodic boundary conditions. The PMMA substrate is modeled using 492 ABAQUS-CPE4HT plane-strain, thermo-mechanically-coupled elements, while the silicon tool is modeled using an appropriately shaped rigid surface. Contact between the substrate and the tool was modeled as frictional, with a Coulomb friction coefficient of 0.75.

SEMimages of the embossed channels in the PMMA at the three different embossing pressures, along with the corresponding numerical simulations are shown in Figure 7. This result nicely shows that the numerical simulations are able to reproduce the process of die-filling as the embossing pressure is increased.

CONCLUDING REMARKS

We have developed a thermo-mechanically-coupled large-deformation isotropic elastic-viscoplastic theory for amorphous polymers in a temperature range which spans their glass transition temperature. The material parameters appearing in the theory have been calibrated for Zeonex-690R, PC, and PMMA

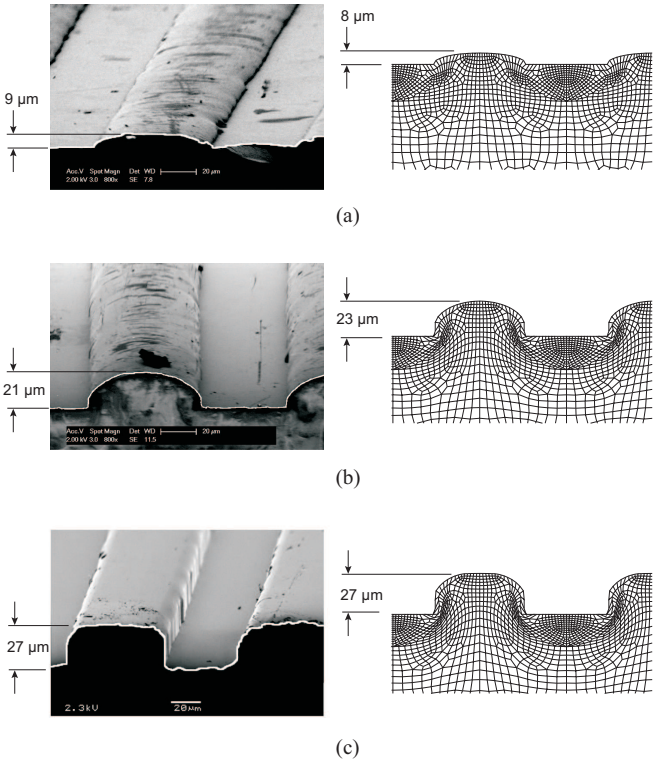

Figure 7. Comparisons of SEM micrographs from micro-hot-embossing experiments on PMMA against corresponding simulations at 130 C, under the following embossing pressures: (a) 0.48 MPa, (b) 1.12 MPa, and (c) 1.6 MPa.

using a relatively complete set of data obtained from constant true strain-rate simple compression experiments in a temperature range from room temperature to $\approx 50\,\mathrm{C}$ above the glass transition temperature, for a variety of strain-rates in the range $\approx 10^{-4}$ to $10^{-1}\,\mathrm{s}^{-1}$, achievable in modern servohydraulic testing machines. The new constitutive theory has been implemented in the finite element program Abaqus/Standard (2009) by writing a user material subroutine. The predictive capabilities of the constitutive theory and its numerical implementation have been validated by comparing the results from a suite of validation experiments against corresponding results from numerical simulations. As demonstrated in this paper, our theory should be useful for modeling important polymer processing operations, such as thermoforming and blow-molding for manufacture of various thin-walled containers, and micro-hot-embossing for the manufacture of microfluidic devices.

REFERENCES

[1] Anand, L., Ames, N., Srivastava, V., and Chester, S., 2009. "A thermo-mechanically-coupled theory for large deformations of amorphous polymers. part i: formulation". *International Journal of Plasticity*, **25**, pp. 1474–1494.

[2] Ames, N., Srivastava, V., Chester, S., and Anand, L., 2009. "A thermo-mechanically-coupled theory for large deformations of amorphous polymers. part ii: applications". *International Journal of Plasticity*, **25**, pp. 1495–1539.

[3] Srivastava, V., Chester, S., and Anand, L., 2010. "A thermo-mechanically-coupled large deformation theory for amorhpous polymers in a temperature range which spans their glass transition". *International Journal of Plasticity*, **26**, pp. 1138–1182.

[4] Srivastava, V., Chester, S., and Anand, L., 2010. "Thermally-actuated shape-memory polymers: experiments, theory, and numerical simulations". *Journal of the Mechanics and Physics of Solids*, **58**, pp. 1100–1124.

[5] Boyce, M., Parks, D., and Argon, A., 1988. "Large inelastic deformation of glassy polymers. part 1: rate dependent constitutive model". *Mechanics of Materials*, **7**, pp. 15–33.

[6] Govaert, L., Timmermans, P., and Brekelmans, W., 2000. "The influence of intrinsic strain softening on strain localization in polycarbonate: modeling and experimental validation". *Journal of Engineering Materials and Technology*, **122**, pp. 177–185.

[7] Anand, L., and Gurtin, M., 2003. "A theory of amorphous solids undergoing large deformations, with applications to polymeric glasses". *International Journal of Solids and Structures*, **40**, pp. 1465–1487.

[8] Buckley, C., and Jones, D., 1995. "Glass-rubber constitutive model for amorphous polymers near the glass transition". *Polymer*, **36**, pp. 3301–3312.

[9] Boyce, M., Socrate, S., and Llana, P., 2000. "Constitutive model for the finite deformation stress-strain behavior of poly(ethylene terephthalate) above the glass transition". *Polymer*, **41**, pp. 2183–2201.

[10] Dooling, P., Buckley, C., Rostami, S., and Zahalan, N., 2002. "Hot-drawing of poly(methyl methacrylate) and simulation using a glass-rubber constitutive model". *Polymer*, **43**, pp. 2451–2465.

[11] Dupaix, R., and Boyce, M., 2007. "Constitutive modeling of the finite strain behavior of amorphous polymers in and above the glass transition". *Mechanics of Materials*, **39**, pp. 39–52.